

Implementation of a time-dependent multiconfiguration self-consistent-field method for coupled electron–nuclear dynamics in diatomic molecules driven by intense laser pulses

Yang Li,^{1,*} Takeshi Sato,^{1,2,3,†} and Kenichi L. Ishikawa^{1,2,3,‡}

¹*Graduate School of Engineering, The University of Tokyo,
7-3-1 Hongo, Bunkyo-ku, Tokyo 113-8656, Japan*

²*Photon Science Center, School of Engineering, University of Tokyo,
7-3-1 Hongo, Bunkyo-ku, Tokyo 113-8656, Japan*

³*Research Institute for Photon Science and Laser Technology,
University of Tokyo, 7-3-1 Hongo, Bunkyo-ku, Tokyo 113-0033, Japan*

We present an implementation of a time-dependent multiconfiguration self-consistent-field (TD-MCSCF) method [R. Anzaki *et al.*, Phys. Chem. Chem. Phys. **19**, 22008 (2017)] with the full configuration interaction expansion for coupled electron-nuclear dynamics in diatomic molecules subject to a strong laser field. In this method, the total wave function is expressed as a superposition of different configurations constructed from time-dependent electronic Slater determinants and time-dependent orthonormal nuclear basis functions. The primitive basis functions of nuclei and electrons are strictly independent of each other without invoking the Born-Oppenheimer approximation. Our implementation treats the electronic motion in its full dimensionality on curvilinear coordinates, while the nuclear wave function is propagated on a one-dimensional stretching coordinate with rotational nuclear motion neglected. We apply the present implementation to high-harmonic generation and dissociative ionization of a hydrogen molecule and discuss the role of electron-nuclear correlation.

I. INTRODUCTION

The rapid development of laser technology enables the generation of coherent light sources that cover a broad frequency range, from the mid infrared, to the X-ray regime [1–5]. The emergence of these new light sources has opened up new opportunities for many scientific fields, such as ultrafast atomic and molecular physics [6–9], attosecond chemistry [10, 11] and material science [12–15] with a goal to visualize, understand and ultimately control electron and nuclear dynamics in atoms, molecules and solids. In particular, when molecules are subject to ultrashort intense laser pulse, the induced molecular dynamics is the simultaneous motion of atomic nuclei and electrons forming a molecular entity [16, 17]. An accurate description of such processes requires treating both electronic and nuclear degrees of freedom on an equal footing. At present, *ab initio* theoretical description of coupled electron-nuclear dynamics in molecules remains challenge.

For the investigation of multielectron dynamics in intense laser fields, the multiconfiguration time-dependent Hartree-Fock (MCTDHF) method has been developed [18–21]. In this approach, the time-dependent total electronic wave function $\Psi(t)$ is given in the configuration interaction (CI) expansion,

$$\Psi(\mathbf{x}_1, \dots, \mathbf{x}_n, t) = \sum_I C_I(t) \Phi_I(\mathbf{x}_1, \dots, \mathbf{x}_n, t), \quad (1)$$

with $\mathbf{x} = \{\mathbf{r}, \sigma\}$ being the spatial-spin variable of the electron. The electronic configuration $\Phi_I(\mathbf{x}_1, \dots, \mathbf{x}_n, t)$ is a Slater determinant constructed from spin orbital functions $\{\psi(\mathbf{r}, t) \times s(\sigma)\}$, where $\{\psi(\mathbf{r}, t)\}$ and $\{s(\sigma)\}$ are electronic spatial orbitals and spin functions, respectively. Both CI coefficients $\{C_I\}$ and orbitals are simultaneously propagated in time, which provides an adequate representation of the temporal change of the wave function with a reduced number of determinants compared to fixed orbital treatment. In the MCTDHF method, the summation in Eq. (1) runs over all possible configurations for a given set of spin orbitals, which are conventionally referred to as full-CI expansion. In the full-CI case, the computational cost due to CI coefficients is proportional to the number of electron distributions among all spin orbitals, which increases factorially with the number of electrons, thus hindering its application beyond small molecular systems. To subjugate this difficulty, variants that go beyond the restriction to the full-CI expansion are now under active development, which we refer to as time-dependent multiconfiguration self-consistent-field (TD-MCSCF) methods [22, 23] in the general case. Representative examples include the time-dependent complete-active-space self-consistent-field (TD-CASSCF) method [24–26], the time-dependent occupation-restricted multiple active-space (TD-ORMAS) method [27, 28] and the time-dependent restricted-active-space self-consistent-field (TD-RASSCF) method [29–31]. These methods are based on the truncated CI expansion within the chosen active orbital space, which are computationally more efficient and at the same time provide compact representation of multielectron dynamics in a given physical condition without sacrificing accuracy.

Efforts have been made to describe the coupled elec-

* yangli@atto.t.u-tokyo.ac.jp

† sato@atto.t.u-tokyo.ac.jp

‡ ishiken@n.t.u-tokyo.ac.jp

tronic and nuclear dynamics of molecules within the framework of the TD-MCSCF method by multiple groups and from diverse perspectives. Nest developed the multiconfiguration electron-nuclear dynamics (MCEND) method [32, 33], where the molecular wave function is represented as a sum over products of determinants for the electrons and Hartree products for the nuclei. By introducing a set of atomic orbitals on "ghost" centers along the internuclear axis of diatomic systems, this method is computationally effective to investigate both electronic and vibrational photo-excitations. However, the MCEND method fails to describe photoionization and dissociation processes due to the use of Gaussian basis functions as electronic basis and limited grid range of nuclear basis [34]. These two processes are keys in understanding the strong coupling of electronic and nuclear dynamics to strong laser fields. Kato and Yamanouchi developed an extended MCTDHF method [35] by using a basis of Slater determinants with time-dependent nuclear orbitals for the fermionic protons while keeping heavy nuclei clamped. This method has been applied to calculate the ground-state properties of a model one-dimensional hydrogen molecule [36], which shows good agreement with the direct solution of the time-dependent Schrödinger equation (TDSE). Very recently, this method has also been adopted for real-time simulation of hydrogen molecular ion (with one electron and one nuclear degree of freedom) irradiated by an intense laser pulse [37]. In another work, Haxton and McCurdy developed a promising way to include quantum treatment of nuclei into MCTDHF for the special case of diatomic molecules. By introducing prolate spheroidal coordinates for the electronic wave function [38], the total wave function is expanded in terms of configurations of orbitals which depend on the internuclear distance. Thus, the trivial but strong correlation between the positions of the nuclei and electrons due to their Coulomb attraction is naturally included and an efficient procedure for evaluating overlap and Hamiltonian matrix elements is formulated. On one hand, geometry-dependent electron orbitals satisfy the key physical condition for the inclusion of strong electron-nuclear coupling. It is demonstrated that such treatment provides a rapidly convergent representation of the vibrational states of diatomics such as HD^+ , H_2 , HD and LiH . On the other hand, the parametric dependence of electron orbitals on the nuclear geometry causes qualitative failure in calculating the dissociative photoionization cross section of H_2^+ [39]. Some alternatives of the prolate spheroidal coordinates have been suggested to resolve this issue. In a series of papers [40–43], Alon and Cederbaum have formulated a multiconfiguration method to describe systems consisting of different types of identical particles with particle conversion taken into account. Stepping forward in this direction, a fully general TD-MCSCF method [44] has been developed in our group, which can describe the dynamics of a many-body system comprising any arbitrary kinds and numbers of fermions and bosons subject to

an external field. The equations of motion (EOMs) of CI-coefficients and spin orbitals are derived for general configuration spaces, based on the time-dependent variational principle. In particular, working equations for molecules subject to intense laser field are formulated in a very flexible manner, without restriction to the full-CI case, and nuclei can be treated as either classical or quantum particles.

In this paper, as the first step towards the numerical implementation of the general TD-MCSCF method [44], we report our implementation specializing for diatomic molecules in the full-CI case. By transforming to Jacobian coordinates and neglecting the rotational motion of the nuclei, we have only one degree of freedom for the nuclear motion. Thus nuclear orbitals can be defined as functions of internuclear distance. This treatment highly simplifies the underlying numerical procedures and at the same time retains the electron-nuclear correlation. For the electron motion, we use three-dimensional curvilinear coordinates to effectively reduce the computational cost. We apply the present implementation to a hydrogen molecule in intense laser fields. By comparing with the clamped-nuclei case, we address the importance of electron-nuclear correlation.

This paper is organized as follows. In Sec. II, we present EOMs of the TD-MCSCF method specialized to diatomic molecules. Numerical implementation is described in Sec. III, and its applications to H_2 and D_2 are described in Sec. IV. Section V concludes this work. Atomic units are used throughout unless otherwise stated.

II. THEORY

A. The system Hamiltonian

We consider a neutral diatomic molecule with N electrons exposed to a laser field linearly polarized parallel with the molecular axis in the z direction. The motions of the two nuclei [with mass and charge (M_1, Z_1) and (M_2, Z_2)] and N electrons are characterized by their position vectors \mathbf{R}_1 , \mathbf{R}_2 , and $\{\mathbf{r}_i' : i = 1, 2, \dots, N\}$, respectively, in the laboratory frame. Hiskes [45] has shown that it is possible to separate the center-of-mass motion by choosing the center of mass of the two nuclei as the origin (Jacobian coordinates [46]) and introducing $N + 2$ new variables: a center-of-mass coordinate \mathbf{R}_c , a relative nuclear coordinate \mathbf{R} and N additional coordinates $\{\mathbf{r}_i : i = 1, 2, \dots, N\}$ representing the position vectors of the i -th electron from the center of mass of the two nuclei. For aligned molecules, we neglect the nuclear rotation and retain only vibrational motion. In this case, the internuclear distance vector \mathbf{R} can be simply expressed as $\mathbf{R} \equiv R\mathbf{e}_z$, where \mathbf{e}_z is the unit vector in the z direction. After several algebraic manipulations (see e.g.,

Ref. [35]), the Hamiltonian for the internal motion reads

$$\hat{H}(t) = \hat{H}^{(n)}(t) + \hat{H}^{(e)}(t) + \hat{H}^{(\text{ne})}, \quad (2)$$

where $\hat{H}^{(n)}(t)$, $\hat{H}^{(e)}(t)$ and $\hat{H}^{(\text{ne})}$ are nuclear part, electronic part of the Hamiltonian and electron-nuclear Coulomb interaction, respectively. $\hat{H}^{(n)}(t)$ describes the relative motion of the two nuclei with the repulsive Coulomb potential and the coupling with the laser field. Within the dipole approximation, it is given by

$$\hat{H}_{\text{LG}}^{(n)}(t) = -\frac{1}{2\mu_n} \frac{\partial^2}{\partial R^2} + \frac{Z_1 Z_2}{R} - \frac{Z_1 M_2 - Z_2 M_1}{M_1 + M_2} E(t) R, \quad (3)$$

in the length gauge (LG), and

$$\hat{H}_{\text{VG}}^{(n)}(t) = -\frac{1}{2\mu_n} \frac{\partial^2}{\partial R^2} + \frac{Z_1 Z_2}{R} - i \frac{Z_1 M_2 - Z_2 M_1}{M_1 M_2} A(t) \frac{\partial}{\partial R}, \quad (4)$$

in the velocity gauge (VG), where $\mu_n = \frac{M_1 + M_2}{M_1 M_2}$ is the reduced nuclear mass, and $E(t)$ and $A(t) = -\int_{-\infty}^t E(t') dt'$ are laser electric field and vector potential, respectively. The last terms in Eq. (3) and (4) vanish for homonuclear molecules such as H_2 because there is no dipole coupling with the laser field for the nuclei. The electronic part of the Hamiltonian in Eq. (2) reads

$$\begin{aligned} \hat{H}^{(e)}(t) = & \sum_{i=1}^N \hat{h}^{(e)}(\mathbf{r}_i, t) + \sum_{i=1}^N \sum_{j>i} \hat{U}^{(\text{ee})}(\mathbf{r}_i, \mathbf{r}_j) \\ & + \sum_{i=1}^N \sum_{j>i} \hat{U}^{(\text{mp})}(\mathbf{r}_i, \mathbf{r}_j), \end{aligned} \quad (5)$$

with the one-body electronic Hamiltonian either in LG or in VG

$$\hat{h}_{\text{LG}}^{(e)}(\mathbf{r}, t) = -\frac{1}{2\mu_e} \nabla^2 + E(t) z, \quad (6)$$

$$\hat{h}_{\text{VG}}^{(e)}(\mathbf{r}, t) = -\frac{1}{2\mu_e} \nabla^2 - i \left(1 + \frac{Z_1 + Z_2}{M_1 + M_2} \right) A(t) \frac{\partial}{\partial z}, \quad (7)$$

the electron-electron Coulomb interaction

$$\hat{U}^{(\text{ee})}(\mathbf{r}_1, \mathbf{r}_2) = \frac{1}{|\mathbf{r}_1 - \mathbf{r}_2|}, \quad (8)$$

and the mass-polarization term

$$\hat{U}^{(\text{mp})}(\mathbf{r}_1, \mathbf{r}_2) = \frac{1}{M_1 + M_2} \nabla_1 \cdot \nabla_2, \quad (9)$$

where $\mu_e = \frac{M_1 + M_2}{M_1 + M_2 + 1}$ is the reduced electron mass. The mass-polarization term Eq. (9) describes the deviation of the center of mass of the nuclei from the center of mass of the nuclei plus any $N - 1$ subset of the N electrons, which is a minor term [47] and omitted in the present

study. Finally, the last term in Eq. (2) represents the electron-nuclear interaction, which has the form

$$\hat{H}^{(\text{ne})}(\mathbf{r}, R) = -\frac{Z_1}{\left| \mathbf{r} + \frac{M_2}{M_1 + M_2} \mathbf{R} \right|} - \frac{Z_2}{\left| \mathbf{r} - \frac{M_1}{M_1 + M_2} \mathbf{R} \right|}. \quad (10)$$

It is worth noting that in the clamped-nuclei model, the electron-nuclear Coulomb interaction is trivially a time-independent quantity which enters to the one-body electron Hamiltonian. However in the quantum-nuclei case, this term is a two-body operator and need to be propagated explicitly.

B. The TD-MCSCF method for the diatomic molecule

In this subsection, we present the TD-MCSCF method [44] specializing for diatomics in the full-CI case. For a compact representation, the formulation of the theory is given in the second quantization formalism. Hereafter, we use orbital indices $\{\mu, \nu, \lambda, \gamma, \delta\}$ for electronic orbitals, $\{p, q, r\}$ for nuclear orbitals, and $\{i, j\}$ for the general (electronic and nuclear) occupied orbitals. For electrons, the Hamiltonian, Eq. (5), can be rewritten as (the mass-polarization term is neglected)

$$\hat{H}^{(e)} = \sum_{\mu, \nu} (h_e)_{\nu}^{\mu} (\hat{E}_e)_{\nu}^{\mu} + \frac{1}{2} \sum_{\mu, \nu, \lambda, \gamma} (g_e)_{\nu\gamma}^{\mu\lambda} (\hat{E}_e)_{\nu\gamma}^{\mu\lambda}, \quad (11)$$

where $(\hat{E}_e)_{\nu}^{\mu} = \sum_{\sigma} \hat{a}_{\mu\sigma}^{\dagger} \hat{a}_{\nu\sigma}$ and $(\hat{E}_e)_{\nu\gamma}^{\mu\lambda} = \sum_{\sigma\sigma'} \hat{a}_{\mu\sigma}^{\dagger} \hat{a}_{\lambda\sigma'}^{\dagger} \hat{a}_{\gamma\sigma'} \hat{a}_{\nu\sigma}$ with $\{\hat{a}_{\mu\sigma}^{\dagger}, \hat{a}_{\mu\sigma} : \sigma \in \uparrow, \downarrow\}$ being the fermionic electron creation and annihilation operators, which change the occupation of spin orbitals $\{\psi_{\mu} \times s(\sigma)\}$ with M_e orthonormal electron spatial functions $\{\psi_{\mu}\}$. The one- and two-electron Hamiltonian matrix elements are defined as

$$(h_e)_{\nu}^{\mu} = \int d\mathbf{r} \psi_{\mu}^*(\mathbf{r}) \hat{h}^{(e)}(\mathbf{r}) \psi_{\nu}(\mathbf{r}), \quad (12)$$

and

$$(g_e)_{\nu\gamma}^{\mu\lambda} = \iint d\mathbf{r}_1 d\mathbf{r}_2 \frac{\psi_{\mu}^*(\mathbf{r}_1) \psi_{\lambda}^*(\mathbf{r}_2) \psi_{\nu}(\mathbf{r}_1) \psi_{\gamma}(\mathbf{r}_2)}{|\mathbf{r}_1 - \mathbf{r}_2|}. \quad (13)$$

Similarly, the operators, Eq. (3), (4) and (10), in the second quantization notation are expressed as

$$\hat{H}^{(n)} = \sum_{p, q} (h_n)_q^p (\hat{E}_n)_q^p, \quad (14)$$

and

$$\hat{H}^{(\text{ne})} = \sum_{p, q, \mu, \nu} (g_{\text{ne}})_{q\nu}^{p\mu} (\hat{E}_n)_q^p (\hat{E}_e)_{\nu}^{\mu}, \quad (15)$$

where $(\hat{E}_n)_q^p = \hat{b}_p^{\dagger} \hat{b}_q$ and $\hat{b}_p^{\dagger}(\hat{b}_p)$ is the nuclear creation (annihilation) operator for the set of M_n nuclear spatial

orbitals $\{\chi_p\}$. The matrix elements, $(h_n)_q^p$ and $(g_{ne})_{q\nu}^{p\mu}$, are defined as

$$(h_n)_q^p = \int dR \chi_p^*(R) \hat{h}^{(n)}(R) \chi_q(R), \quad (16)$$

and

$$(g_{ne})_{q\nu}^{p\mu} = \iint dR d\mathbf{r} \chi_p^*(R) \psi_\mu^*(\mathbf{r}) \hat{H}^{(ne)}(\mathbf{r}, R) \times \chi_q(R) \psi_\nu(\mathbf{r}). \quad (17)$$

For the convenience of later discussion, we define the one- and two-body reduced density matrix (RDM) elements as

$$(\rho_e)_\nu^\mu = \langle \Psi | (\hat{E}_e)_\mu^\nu | \Psi \rangle, \quad (18a)$$

$$(\rho_n)_q^p = \langle \Psi | (\hat{E}_n)_p^q | \Psi \rangle, \quad (18b)$$

$$(\rho_{ee})_{\nu\gamma}^{\mu\lambda} = \langle \Psi | (\hat{E}_e)_{\mu\lambda}^{\nu\gamma} | \Psi \rangle, \quad (18c)$$

$$(\rho_{ne})_{q\nu}^{p\mu} = \langle \Psi | (\hat{E}_n)_p^q (\hat{E}_e)_\mu^\nu | \Psi \rangle, \quad (18d)$$

where Ψ is the total molecular wave function defined below in Eq. (19).

In the TD-MCSCF method limited to full-CI expansion, the total electron-nuclear wave function of a diatomic molecule is expanded as

$$\Psi(t) = \sum_{I,p} C_{I,p}(t) \Phi_I(t) \chi_p(t), \quad (19)$$

where $\{\Phi_I\}$ denotes the N -electron Slater determinants constructed from electronic orbitals $\{\psi_\mu\}$, and $\{\chi_p\}$ are nuclear orbitals.

The EOMs for the TD-MCSCF method have been derived based on the time-dependent variational principle [48, 49], where the action integral S ,

$$S = \int dt \langle \Psi | \hat{H} - i \frac{\partial}{\partial t} | \Psi \rangle, \quad (20)$$

is made stationary with respect to any possible variations of orbitals $\{\psi_\mu\}$ and $\{\chi_p\}$ as well as the CI coefficients $\{C_{I,p}\}$. The detailed derivation has been given in Ref. [44]. Here in our notation, the resulting EOMs of the CI coefficients read

$$i \frac{d}{dt} C_{I,p} = \sum_{J,q} \langle \Phi_I \chi_p | \hat{H} - \hat{X}^{(n)} - \hat{X}^{(e)} | \Phi_J \chi_q \rangle C_{J,q}. \quad (21)$$

The EOMs of the nuclear and electronic orbitals are given by

$$i \frac{\partial}{\partial t} |\chi_i\rangle = \hat{Q}^{(n)} \left\{ \hat{h}^{(n)} |\chi_i\rangle + \sum_{p,q} (\rho_n^{-1})_i^p \sum_{\mu,\nu} (\rho_{ne})_{p\mu}^{q\nu} (\hat{W}_{ne})_\nu^\mu |\chi_q\rangle \right\} + \sum_j |\chi_j\rangle (X_n)_i^j, \quad (22)$$

$$i \frac{\partial}{\partial t} |\psi_i\rangle = \hat{Q}^{(e)} \left\{ \hat{h}^{(e)} |\psi_i\rangle + \sum_{\mu,\nu} (\rho_e^{-1})_i^\mu \left[\sum_{\lambda,\gamma} (\rho_{ee})_{\mu\lambda}^{\nu\gamma} (\hat{W}_e)_\gamma^\lambda + \sum_{p,q} (\rho_{ne})_{p\mu}^{q\nu} (\hat{W}_{en})_q^p \right] |\psi_\nu\rangle \right\} + \sum_j |\psi_j\rangle (X_e)_i^j. \quad (23)$$

In Eq. (21)-(23), the operators $\hat{Q}^{(n)} = 1 - \sum_p |\chi_p\rangle \langle \chi_p|$ and $\hat{Q}^{(e)} = 1 - \sum_\mu |\psi_\mu\rangle \langle \psi_\mu|$ are projectors onto the orthogonal complement of the occupied orbital space, which guarantee the orthonormality of orbitals during time propagation. $(\hat{W}_e)_\nu^\mu$, $(\hat{W}_{ne})_\nu^\mu$ and $(\hat{W}_{en})_q^p$ are mean-field potentials, given, in the coordinate space, by

$$(\hat{W}_e)_\nu^\mu(\mathbf{r}) = \int d\mathbf{r}' \frac{\psi_\mu^*(\mathbf{r}') \psi_\nu(\mathbf{r}')}{|\mathbf{r} - \mathbf{r}'|}, \quad (24)$$

$$(\hat{W}_{ne})_\nu^\mu(R) = \int d\mathbf{r} \psi_\mu^*(\mathbf{r}) \hat{H}^{(ne)}(\mathbf{r}, R) \psi_\nu(\mathbf{r}), \quad (25)$$

and

$$(\hat{W}_{en})_q^p(\mathbf{r}) = \int dR \chi_p^*(R) \hat{H}^{(ne)}(\mathbf{r}, R) \chi_q(R). \quad (26)$$

The operators, $\hat{X}^{(n)}$ and $\hat{X}^{(e)}$, whose matrix elements are defined by

$$(\hat{X}_n)_q^p = i \langle \chi_p | \frac{\partial}{\partial t} | \chi_q \rangle, \quad (27)$$

and

$$(\hat{X}_e)_\nu^\mu = i \langle \psi_\mu | \frac{\partial}{\partial t} | \psi_\nu \rangle, \quad (28)$$

determine the components of the time derivation of the orbitals within the occupied orbital space. These two operators impose constraints to the EOMs, which can be arbitrary Hermitian matrices. Depending on the choice of the constraint operators, the EOMs have various equivalent forms. In the present study, we choose the natural-orbital constraint, i.e., the form the constraint operators

$\hat{X}^{(n)}$ and $\hat{X}^{(e)}$ satisfies the condition to diagonalize the one-body RDMs for both electrons and nuclei [50]. In other words, electronic and nuclear natural orbitals [51] are propagated directly during the interaction with the laser pulse. This form is particularly suited for our propagation scheme applied below. Explicit expressions for the natural-orbital constraint operators together with their variants in imaginary-time propagation for ground-state calculation are given in Appendix A. For completeness, we also briefly summarize the working equations of TD-MCSCF method for a pure multielectron system within clamped nuclei in Appendix B.

III. IMPLEMENTATION

One of the important aspects for the implementation of TD-MCSCF method using real-space grid-based techniques is the choice of coordinate system. Many existing implementations of TD-MCSCF method are optimized to efficiently study the strong-field phenomena in atoms and diatomic molecules in the presence of either linearly- or elliptically-polarized laser pulse, exploiting the underlying symmetries of the system Hamiltonian with, for instance, the spherical [25, 26, 28, 52], cylindrical [37], or prolate spheroidal coordinates [38]. To retain the possibility of carrying out first-principle simulations of the response of molecules to intense laser pulses without assuming symmetry, we do not pursue this direction here.

The most straightforward way is using Cartesian coordinate with an equal grid mesh. While this approach offers better opportunities for parallel computing due to the highly sparse and structured representation of the Hamiltonian, it suffers from drawbacks of requiring small grid spacings to accurately represent the electron-nucleus interaction and a large number of grid points to sustain photoelectrons (or dissociated nuclei). One way to overcome this problem is using multi-resolution Cartesian grid [53], which has previously been demonstrated for the implementation of MCTDHF method. Alternatively, we can use curvilinear coordinates [54–56]. By choosing an appropriate coordinate transformation, it is possible to achieve a high spatial resolution in the vicinity of nuclei and, at the same time, a sufficiently large simulation box. Furthermore, the coordinate transformation can be given in analytical form. Accompanying with this, the EOMs can be analytically transformed. The transformed EOMs are discretized using higher-order finite difference methods on *an equal grid mesh* in curvilinear coordinates. Such a treatment overcomes the shortcomings of equal grid mesh while retaining its advantages. This scenario is demonstrated for the implementation of the time-dependent Hartree-Fock (TDHF) method elsewhere. In Sec. III A, we describe the coordinate transformation for the present case.

Another important issue is the time propagation method. The orbital EOMs Eq. (22) and (23) consist of stiff linear terms and nonstiff nonlinear terms. The

stiffness of the linear part comes from the one-body kinetic energy operators while the nonlinear terms contain dependencies on the CI coefficients and the orbitals. For an efficient propagation of the EOMs, we adopt the exponential time differencing second-order Runge-Kutta scheme (ETDRK2) [57, 58], as described in Sec. III B.

A. Curvilinear Coordinate

Here we mainly focus on the electron coordinate transformation and briefly mention the nuclear transformation at the end of this subsection. Let us consider the physical space to be described by Cartesian coordinates $\mathbf{r} = (x, y, z) = (r_1, r_2, r_3)$ and an analytical transformation $\mathbf{r} = \mathbf{f}(\boldsymbol{\xi})$ to curvilinear coordinates $\boldsymbol{\xi} = (\xi_1, \xi_2, \xi_3)$ that act as the computational space. This transformation is single-valued and at least twice continuously differentiable on a three-dimensional domain. The Jacobian of the transformation \mathbf{J} is defined as a 3×3 matrix of which the (i, j) matrix element is $J_j^i = \partial r_i / \partial \xi_j$, with $|J| = \det \mathbf{J}$ being its determinants. The metric tensor g_j^i in the curvilinear coordinates is

$$g_j^i = \sum_{k=1}^3 (J^{-1})_k^i (J^{-1})_k^j = \sum_{k=1}^3 \frac{\partial \xi_i}{\partial r_k} \frac{\partial \xi_j}{\partial r_k}, \quad (29)$$

and the Laplacian operator is given by

$$\nabla^2 = \sum_{i=1}^3 \sum_{j=1}^3 \frac{1}{|J|} \frac{\partial}{\partial \xi_i} |J| g_j^i \frac{\partial}{\partial \xi_j}. \quad (30)$$

It is beneficial to transform the electron orbitals as

$$\tilde{\psi}_\mu(\boldsymbol{\xi}) = \sqrt{|J|} \psi_\mu(\mathbf{r}(\boldsymbol{\xi})), \quad (31)$$

such that the inner product obeys

$$\int d\mathbf{r} \psi_\mu^*(\mathbf{r}) \psi_\nu(\mathbf{r}) = \int d\boldsymbol{\xi} \tilde{\psi}_\mu^*(\boldsymbol{\xi}) \tilde{\psi}_\nu(\boldsymbol{\xi}). \quad (32)$$

Inserting Eq. (31) into Eq. (23), any electron operator \hat{h} in the EOMs of transformed electron orbitals will change according to $\hat{h} \rightarrow \sqrt{|J|} \hat{h} \frac{1}{\sqrt{|J|}}$. For example, the transformed Laplacian reads

$$\sqrt{|J|} \nabla^2 \frac{1}{\sqrt{|J|}} = \sum_{i=1}^3 \sum_{j=1}^3 \frac{1}{\sqrt{|J|}} \frac{\partial}{\partial \xi_i} |J| g_j^i \frac{\partial}{\partial \xi_j} \frac{1}{\sqrt{|J|}}, \quad (33)$$

and z component of the transformed momentum operator is expressed as

$$-i\sqrt{|J|} \frac{\partial}{\partial z} \frac{1}{\sqrt{|J|}} = -\frac{i}{2} \sum_{j=1}^3 \left(\frac{\partial \xi_j}{\partial z} \frac{\partial}{\partial \xi_j} + \frac{\partial}{\partial \xi_j} \frac{\partial \xi_j}{\partial z} \right). \quad (34)$$

The electron mean-field potential Eq. (24) is evaluated by solving the corresponding Poisson equation

$$\nabla^2 (\hat{W}_e)_\nu^\mu(\mathbf{r}) = -4\pi \psi_\mu^*(\mathbf{r}) \psi_\nu(\mathbf{r}). \quad (35)$$

Defining $(\hat{W}'_e)^\mu_\nu(\xi) = \sqrt{|J|}(\hat{W}_e)^\mu_\nu(\mathbf{r}(\xi))$, in the same way as in Eq. (31), the Poisson equation is transformed as

$$\sqrt{|J|}\nabla^2 \frac{1}{\sqrt{|J|}}(\hat{W}'_e)^\mu_\nu(\xi) = -4\pi\sqrt{|J|}\tilde{\psi}_\mu^*(\xi)\tilde{\psi}_\nu(\xi). \quad (36)$$

With all the transformed operators available, the transformed EOMs can be discretized on the computational space $\xi = (\xi_1, \xi_2, \xi_3)$ by equally spaced grids. The fifth-order central finite difference is applied for spatial differential operators. To incorporate the exterior complex scaling (ECS) absorbing boundary [26, 59–62], we use an orthogonal transformation

$$r_i = f(\xi_i), \quad i = 1, 2, 3, \quad (37)$$

which smoothly scales the real ξ_i to complex r_i . The explicit expression for this transformation reads

$$f(\xi) = \begin{cases} \Delta_t e^{i\theta}(\xi + \xi^{(1)}) - \xi^{(2)} & (\xi < -\xi^{(1)}) \\ \Delta_s \xi - \sum_{p=5}^8 b_p(\xi^{(1)} - \xi^{(0)})^{8-p}(\xi + \xi^{(0)})^p & (-\xi^{(1)} \leq \xi < -\xi^{(0)}) \\ \Delta_s \xi & (-\xi^{(0)} \leq \xi \leq \xi^{(0)}) \\ \Delta_s \xi + \sum_{p=5}^8 a_p(\xi^{(1)} - \xi^{(0)})^{8-p}(\xi - \xi^{(0)})^p & (\xi^{(0)} < \xi \leq \xi^{(1)}) \\ \Delta_t e^{i\theta}(\xi - \xi^{(1)}) + \xi^{(2)} & (\xi^{(1)} < \xi) \end{cases} \quad (38)$$

where the computational space along one direction are divided into five regions: the inner region $(-\xi^{(0)} \leq \xi \leq \xi^{(0)})$, two intermediate regions $(-\xi^{(1)} \leq \xi < -\xi^{(0)})$ and $(\xi^{(0)} < \xi \leq \xi^{(1)})$ and two out regions $(\xi < -\xi^{(1)})$ and $(\xi^{(1)} < \xi)$. The parameters Δ_s and Δ_t are the scaling factors in the inner and outer regions, respectively. The polynomials are used in the intermediate regions, where parameters a_p and $b_p = (-1)^p a_p$ are determined to satisfy the conditions of continuity of $f(\xi)$ and its first and second derivatives at the boundaries. θ is the ECS scaling angle.

Special care should be taken for solving Poisson equation when analytic continuation is applied for the orbitals. In this case, solving Poisson equation in the complex-scaled region ($|\xi| > \xi^{(0)}$) turns out to be numerically unstable [26]. In the present study, we approximately neglect the Coulomb interaction between electrons in the scaled region and adopt *octupole* expansion for the calculation of electron mean-field potential in the scaled region as well as the boundary condition of solving Poisson equation in the unscaled region.

The nuclear coordinate is transformed in a similar way as that of electrons, i.e., $R = f(\zeta)$, together with orbital transformation $\tilde{\chi}_p(\zeta) = \sqrt{f'}\chi_p(\zeta)$. The transformed EOMs of nuclear orbitals are numerically discretized on equally spaced points in ζ and readily propagated. Same transformation function in Eq. (38) is adopted except for the condition $\zeta > 0$.

B. Time propagation scheme

We rewrite the electronic orbital EOMs Eq. (23) as a nonlinear differential equation

$$\frac{\partial}{\partial t}u(t) = -i\hat{h}u(t) + N[t, u(t)], \quad (39)$$

where \hat{h} is a stiff linear operator and $N[t, u(t)]$ a nonstiff nonlinear reminder. We first consider the stiff part to be time-independent, i.e., $\hat{h} = -\frac{1}{2\mu_e}\nabla^2$, and put the laser interaction term into nonlinear part. Eq. (39) can be integrated over a small time interval $[t_n, t_{n+1} = t_n + \Delta t]$ as

$$u(t_{n+1}) = e^{-i\hat{h}\Delta t}u(t_n) + \int_{t_n}^{t_{n+1}} dt' e^{i\hat{h}(t_{n+1}-t')} N[t', u(t')], \quad (40)$$

which is exact for time-independent \hat{h} . This scheme is called the exponential integrator [58]. By approximating $N[t', u(t')]$ in the integrand using second-order Runge-Kutta (RK2) method, we obtain the expressions of ET-DRK2 method

$$a(t_n) = u(t_n) + \Delta t \varphi_1 \left(-i\hat{h}(t_n)\Delta t \right) \times \left\{ -i\hat{h}(t_n)u(t_n) + N[t_n, u(t_n)] \right\}, \quad (41)$$

and

$$u(t_{n+1}) = a(t_n) + \Delta t \varphi_2 \left(-i\hat{h}(t_n)\Delta t \right) \times \left\{ N[t_{n+1}, a(t_n)] - N[t_n, u(t_n)] \right\}, \quad (42)$$

where the φ -functions are defined as

$$\varphi_1(z) = \frac{e^z - 1}{z}, \quad \varphi_2(z) = \frac{e^z - 1 - z}{z^2}. \quad (43)$$

We use the *expokit* package [63] to efficiently calculate the action of φ functions on the operand vectors in Eq. (41) and (42). The modification for time-dependent stiff operator $\hat{h}(t)$ is given in Appendix C. The nuclear EOMs Eq. (22) are propagated in the same manner. For CI EOMs Eq. (21), we treat the totality of r.h.s as nonlinear term and time propagation of CI reduces to RK2 scheme.

IV. NUMERICAL RESULTS AND DISCUSSIONS

A. Ground-state properties of H₂

To assess the performance of the method and our implementation described in Sec. II and III, we first do a series of ground-state calculations taking the H₂ molecule as an example, either with clamped-nuclei approximation or fully quantum mechanically with nuclear motion

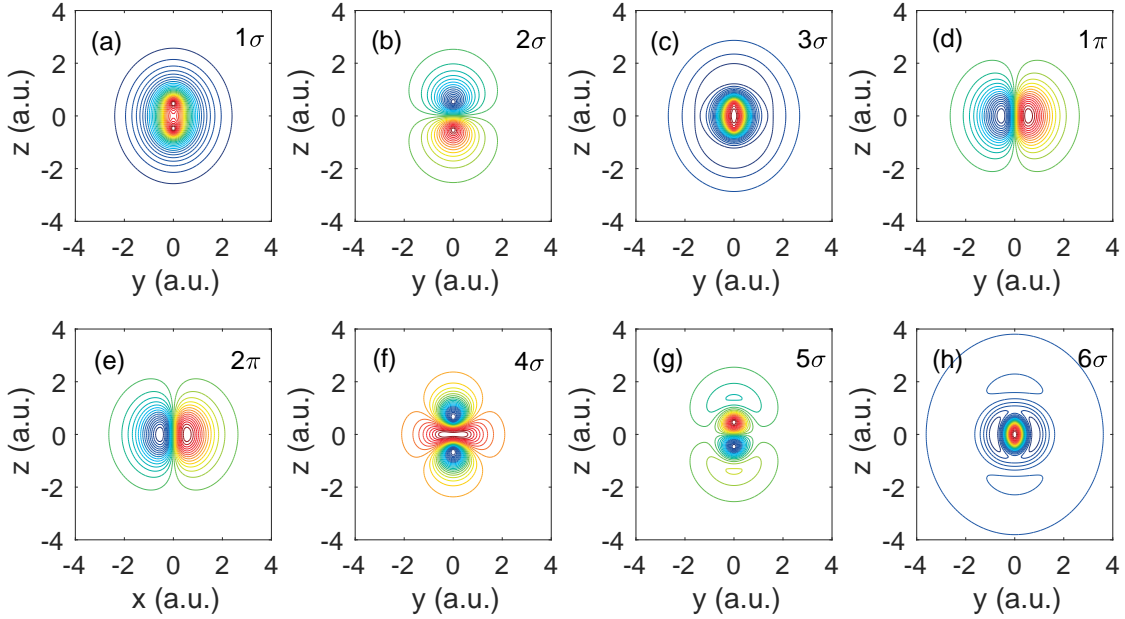


FIG. 1. Electronic natural orbitals of ground state H_2 with fixed nuclei. The orbital space is $6\sigma 2\pi$. The molecule is aligned along z -axis. Except for panel (e), where the orbital slice is plotted in xz -plane, all the other orbitals are shown in yz -plane.

(hereafter refer to as quantum-nuclei). We assume a H_2 molecule is aligned along z -axis. The imaginary-time propagation method is adopted to obtain the ground state. The grid resolution is optimized for ground-state calculations in order to have a better comparison with the existing literature values of ground-state properties such as ground-state energy and natural occupation number. In the quantum-nuclei case, we use $\Delta\xi = 0.08$ a.u. and box size of $\xi_{\max} = 8$ a.u. for all the three directions of the electronic coordinates, and $\Delta\zeta = 0.05$ a.u. and total length of $\zeta_{\max} = 6$ a.u. for nuclear coordinate. Curvilinear transformation is not used in this subsection. In the clamped-nuclei case, the same spatial grid is used for electrons, and nuclei are fixed at equilibrium internuclear distance $R = 1.4$ a.u.

Let us first consider the case of the clamped-nuclei H_2 molecule. In Table I, we present the ground state energies for different numbers M of electron orbitals. Up to eight orbitals with six σ and two degenerate π orbitals are used. Clearly, with increasing M , the ground-state energy consistently converges to the exact value [64] obtained by the direct solution of two-electron Schrödinger equation, and only a few orbitals are needed to obtain good agreement. The energy values in this work (third column) have a higher precision than those from Ref. [53] (fourth column) due to finer spatial resolution. For instance, the Hartree-Fock energy presented here is nearly identical to that calculated using the finite-element discrete variable representation basis set in Ref. [38]. In the fifth column, we also give the fraction of the correlation energy defined as $F_c(M) = [E(M) - E(1)] / [E_{\text{exact}} - E(1)]$. In

TABLE I. Clamped-nuclei H_2 ground-state energies for different numbers M of electron orbitals and the fraction of the covered electron-electron correlation energy. The reference energy values are taken from Ref. [53] calculated by the MCTDHF method using a multi-resolution Cartesian grid. The exact energy is taken from Ref. [64] by directly solving two-electron Schrödinger equation. The equilibrium internuclear distance of H_2 is $R = 1.4$ a.u. The nuclear Coulomb repulsion energy is excluded in the ground-state energy.

No. of orbitals M	Orbital space	Energy [a.u.]		Correlation [%]
		This work	Ref. [53]	
1 (HF)	1σ	-1.84792	-1.84123	0.00
2	2σ	-1.86644	-1.85964	45.35
3	3σ	-1.87390	-1.86723	63.61
5	$3\sigma 2\pi$	-1.88436	N/A	89.23
6	$4\sigma 2\pi$	-1.88488	-1.87756	90.50
7	$5\sigma 2\pi$	-1.88538	N/A	91.72
8	$6\sigma 2\pi$	-1.88566	N/A	92.41
Exact		-1.88876		100.00

the most accurate case $M = 8$, 92.41% of the correlation energy is recovered.

The total wave function $\Psi(t)$ of clamped-nuclei H_2 molecule can be expressed by using different types of electron orbitals. In the present work, we use natural-orbital representation as explained in Appendix A, where the one-body RDM is kept diagonal during the propagation. In this way, natural orbitals and natural occupation numbers, defined as eigenvectors and eigenvalues of the one-body RDM, are directly obtained after the propagation. Taking $M = 8$ for example, we present the natural

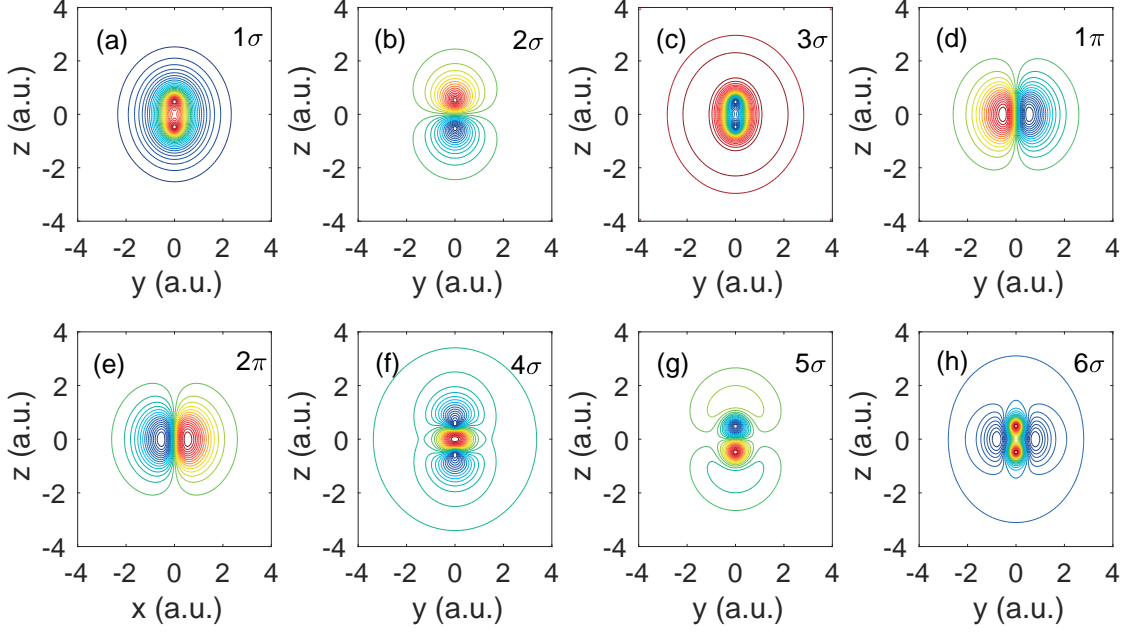


FIG. 2. Electronic natural orbitals of ground state quantum-nuclei H_2 . Same number of electronic and nuclear orbitals $M = 8$ is used with electronic orbital space $6\sigma 2\pi$.

TABLE II. Natural occupation numbers of a clamped-nuclei H_2 molecule for $M = 8$. The orbital space is $6\sigma 2\pi$. The results are listed in descending order. The reference values from Ref. [38] are also given for comparison. Note that there are typos for the occupation numbers of 4σ and 5σ orbitals in Ref. [38], which have been corrected in this table.

Orbital	Natural occupation number	
	This work	Ref. [38]
1σ	1.96330	1.96
2σ	2.09560×10^{-2}	2.10×10^{-2}
3σ	6.34418×10^{-3}	6.34×10^{-3}
1π	4.46415×10^{-3}	4.46×10^{-3}
2π	4.46415×10^{-3}	4.46×10^{-3}
4σ	2.03040×10^{-4}	2.03×10^{-4}
5σ	1.90875×10^{-4}	1.91×10^{-4}
6σ	8.36366×10^{-5}	8.36×10^{-5}

occupation numbers in Table II. The natural occupation numbers represent the distribution of all electrons among natural orbitals. Their sum is equal to the number of electrons (2 for a hydrogen molecule). As can be seen, the first natural orbital is highly occupied with an occupation number close to two while for higher orbitals the occupation numbers decrease rapidly. The two degenerate π orbitals have exactly the same occupation numbers, as expected. Our results are in excellent agreement with those in Ref. [38] calculated by prolate spheroidal coordinate code, validating our implementation. The two dimensional slices of natural orbitals are displayed in Fig 1, where orbital symmetries can be clearly iden-

TABLE III. Quantum-nuclei H_2 ground-state energies for different numbers M of electronic and nuclear orbitals and the fraction of the covered correlation energy. The exact energy is taken from Ref. [65].

No. of orbitals M	Electronic orbital space	Energy [a.u.]	Correlation [%]
1	1σ	-1.11519	0.00
2	2σ	-1.13434	39.21
3	3σ	-1.14746	66.07
5	$3\sigma 2\pi$	-1.15770	87.04
6	$4\sigma 2\pi$	-1.15937	90.46
7	$5\sigma 2\pi$	-1.16014	92.04
8	$6\sigma 2\pi$	-1.16062	93.02
Exact		-1.16403	100.00

tified. The information of orbital symmetries can guide us to study the time-evolution behavior of the orbitals in the response to the laser field. For instance, the two π orbitals in Fig 1(d) and 1(e) will respond in the same fashion to a laser field polarized parallel to the molecular axis.

Next, we examine the ground-state properties of quantum-nuclei H_2 molecule. In the present study, we always use the same number of electronic and nuclear orbitals, i.e., $M_e = M_n \equiv M$, although this is not a necessary constraint for this system [50]. The nuclear masses of H_2 are set to $M_1 = M_2 = 1836.15$ a.u. The ground-state energies with respect to M are shown in Table III. Similar to the clamped-nuclei case, the ground-state energy monotonically tends to the exact value [65] with an

TABLE IV. Electronic and nuclear natural occupation numbers of a quantum-nuclei H_2 molecule for $M = 8$. The electronic orbital space is $6\sigma 2\pi$. The results are listed in descending order. The reference values of electronic natural orbitals are taken from Ref. [38].

Orbital		Natural occupation number		
Nuclear	Electronic	Nuclear	Electronic	Ref. [38]
1	1σ	9.968×10^{-1}	1.953	1.95
2	2σ	3.166×10^{-3}	2.348×10^{-2}	2.35×10^{-2}
3	3σ	1.034×10^{-5}	1.407×10^{-2}	1.46×10^{-2}
4	1π	3.227×10^{-8}	4.456×10^{-3}	4.43×10^{-3}
5	2π	7.108×10^{-10}	4.456×10^{-3}	4.43×10^{-3}
6	4σ	7.098×10^{-11}	5.990×10^{-4}	6.18×10^{-4}
7	5σ	2.382×10^{-11}	3.496×10^{-4}	3.47×10^{-4}
8	6σ	3.575×10^{-12}	2.832×10^{-5}	1.82×10^{-4}

increasing number of orbitals. 93.02% of the correlation energy is accounted at $M = 8$. The nuclear and electronic natural occupation numbers for $M = 8$ are presented in Table IV, with reference values from Ref. [38] for comparison. The corresponding electronic natural orbitals are shown in Fig. 2. We see in Fig. 1 and Fig. 2 that the overall shapes of the two sets of natural orbitals are remarkably similar, although small differences can be viewed, for instance, in the 4σ and 6σ orbitals. Unlike the treatment in Ref. [38], where the electron orbitals have parametric dependence on nuclear coordinate R through the prolate spheroidal coordinate system, in our electron-nuclear wave function expansion Eq. (19), the electronic and nuclear primitive orbital functions are strictly independent without parametric dependence. The similarity of the natural orbitals in Fig. 1 and Fig. 2 thus suggests that the strong correlation between the positions of the nuclei and electrons due to their Coulomb attraction are correctly accounted in our calculation.

B. Electron-nuclear dynamics of H_2 in an intense laser field

In this subsection, we present numerical applications of the implementation of our method to H_2 subject to an intense laser pulse linearly polarized along the molecular axis in the z direction, both in fixed-nuclei and quantum-nuclei case. We adopt VG and assume the vector potential of the laser field of the following form:

$$A(t) = \frac{\sqrt{I_0}}{w} \sin^2\left(\frac{\pi t}{N_0 T}\right) \sin \omega t, \quad 0 \leq t \leq N_0 T, \quad (44)$$

where I_0 is the peak intensity, T the laser period, $\omega = 2\pi/T$ the angular frequency and N_0 the total number of laser optical cycles.

For time-dependent calculations, a grid width larger than that used in the ground state calculation is employed so that the computational time falls in an affordable range. We use grid spacing $\Delta\xi = 0.2$ a.u. for

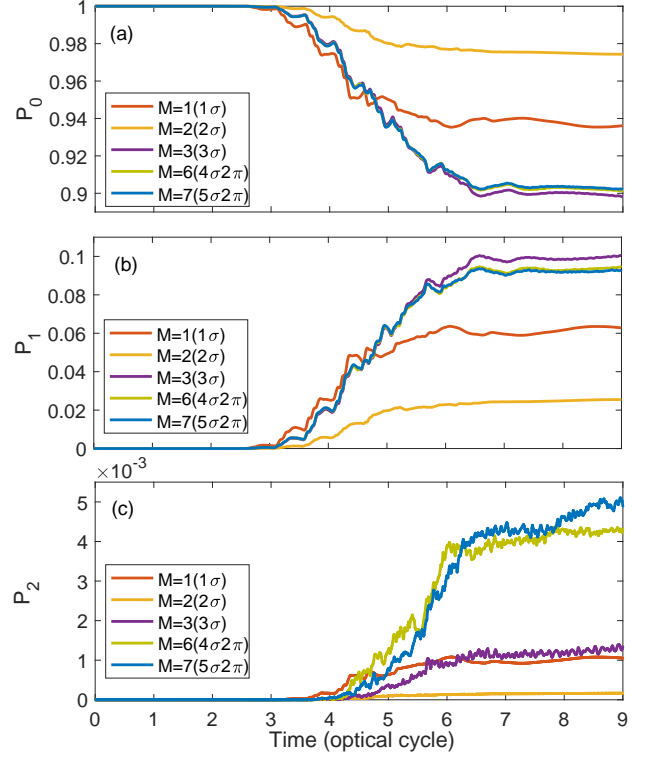


FIG. 3. Time evolution of (a) survival probability, (b) single-ionization probability, and (c) double-ionization probability of a clamped-nuclei H_2 molecule exposed to an infrared laser pulse with a wavelength of 800 nm, an intensity of $3 \times 10^{14} \text{ W/cm}^2$ and a foot-to-foot duration of 8 optical cycles. Results of the TD-MCSCF (or MCTDHF) method are obtained with different numbers M of electron orbitals.

all the three directions of the electronic coordinates and $\Delta\zeta = 0.08$ a.u. for the nuclear coordinate. The scaling factors in the curvilinear transformation Eq. (38) are chosen to be $\Delta_s = 1$ and $\Delta_t = 5$ and the ECS scaling angle is set to $\theta = 15^\circ$. Other parameters in Eq. (38) for the electronic and nuclear coordinates are listed in Table V. The ETDRK2 method described in the previous section is used to propagate EOMs with 10 000 time steps per optical cycle. We have confirmed the convergence of the results with respect to spatial and temporal resolutions.

We first simulate a clamped-nuclei H_2 molecule subject to a near infrared laser field with a wave length of 800 nm, $3 \times 10^{14} \text{ W/cm}^2$ intensity and total duration of 8 optical cycles. For such a process, the direct exact numerical solution of the six-dimensional TDSE is still unavailable to our knowledge, due to the unfavorable scaling of the problem size with the laser wavelength. So we choose the result of the largest configuration space considered in our time-dependent simulation, $M = 7$, as a reference. The simulation results are shown in Figs. 3 and 4. We present here the time evolution of the n -electron ionization probability (Fig. 3) and the HHG spectra (Fig. 4). The n -electron ionization probability, P_n ($n = 0, 1, 2$),

TABLE V. Coordinate transformation parameters in Eq. (38) for electronic and nuclear coordinates

Parameter	Nucleus	Electron		
	$\zeta \rightarrow R$	$\xi_1 \rightarrow x$	$\xi_2 \rightarrow y$	$\xi_3 \rightarrow z$
$\xi^{(0)}$	20	10	10	60
$\xi^{(1)}$	30	18	18	80
$\xi^{(2)}$	$49.15 + 6.47i$	$33.32 + 5.18i$	$33.32 + 5.18i$	$118.30 + 12.94i$
a_5	$(2.68 + 0.91i) \times 10^{-6}$	$(1.27 + 0.43i) \times 10^{-5}$	$(1.27 + 0.43i) \times 10^{-5}$	$(2.09 + 0.71i) \times 10^{-8}$
a_6	$(-5.36 - 1.81i) \times 10^{-6}$	$(-2.56 - 0.86i) \times 10^{-5}$	$(-2.56 - 0.86i) \times 10^{-5}$	$(-4.19 - 1.42i) \times 10^{-8}$
a_7	$(3.83 + 1.29i) \times 10^{-6}$	$(1.83 + 0.62i) \times 10^{-5}$	$(1.83 + 0.62i) \times 10^{-5}$	$(2.99 + 1.01i) \times 10^{-8}$
a_8	$(-9.57 - 3.24i) \times 10^{-7}$	$(-4.57 - 1.54i) \times 10^{-6}$	$(-4.57 - 1.54i) \times 10^{-6}$	$(-7.48 - 2.53i) \times 10^{-9}$

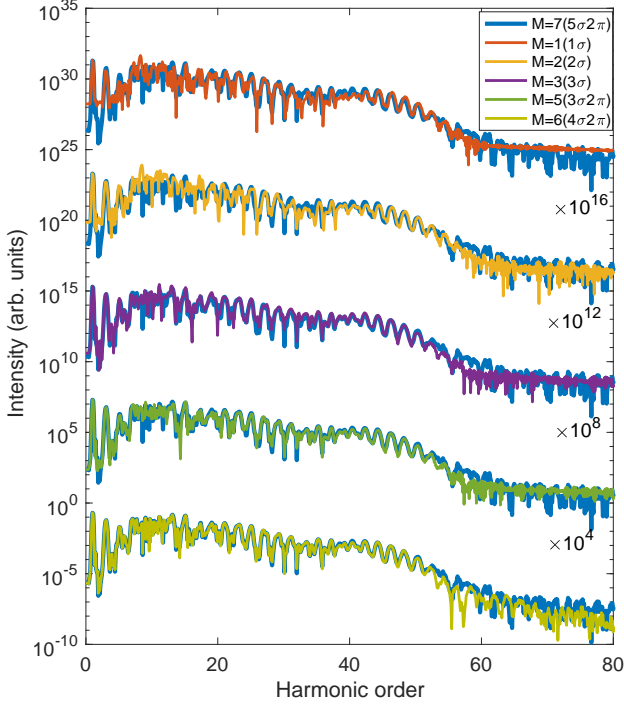


FIG. 4. High-harmonic spectra of a clamped-nuclei H_2 molecule irradiated by an infrared laser pulse with a wavelength of 800 nm, an intensity of $3 \times 10^{14} \text{ W/cm}^2$ and a foot-to-foot duration of 8 optical cycles. Result of TD-MCSCF (or MCTDHF) method with 7 ($5\sigma + 2\pi$) orbitals works as a reference. Other results with different numbers of orbitals are compared to it. The curves are vertically shifted for clarity.

is conveniently defined as a probability to find n electrons located outside a cube with a side length of 10 a.u., which can be evaluated using the method introduced in Ref. [24]. The HHG spectra are obtained as the modulus squared of the Fourier transform of the dipole acceleration, which, in its turn, is evaluated by double numerical differentiation of the dipole moment with respect to time. Figure 3 plots the survival probability P_0 , the single-ionization probability P_1 , and double-ionization probability P_2 with different number of orbitals, respectively.

While P_0 and P_1 are converged for $M \geq 3$, the results with $M = 1$ and 2 show strong underestimations, which indicates the electron correlation plays a nonnegligible role during the interaction with the laser pulse. For the double ionization probability, in great contrast, we can see from Fig. 3(c) that it is not fully converged even with $M = 7$ and still varies after the end of the laser pulse ($t > 8T_0$). This observation indicates that the double ionization is much more sensitive to the electron-electron correlation than single ionization and HHG (see below) [66, 67]. The high-harmonic spectra calculated with different numbers of orbitals are shown in Fig. 4. The TDHF ($M = 1$) result already provides the correct cutoff position but underestimates the harmonic intensity in the plateau region. As the number of orbitals is increased, the TD-MCSCF method provides improved description of electron-electron correlation, and thus the harmonic spectrum displays a fairly rapid convergence with respect to M . In particular, HHG spectra with $M = 6$ and $M = 7$ show remarkable agreement with each other on the scale of the figure.

Next, let us turn to the quantum-nuclei case. The laser parameters are the same as in the clamped-nuclei case. We first analyze the time-dependent nuclear probability density, defined as the modulus squared of the total wave function integrated over the electronic coordinates. Fig 5 shows the logarithmically scaled, time-dependent nuclear probability density. The simulations are continued for 20 optical cycles in order to fully record the time evolution of the nuclear wave packet. In the case of $M = 1$, only vibrational motion around the equilibrium internuclear distance shows up. In the TD-MCSCF calculation with $M = 2$, higher order vibrational components appear. For $M = 5$, even stronger vibration is seen, whereas the dissociation is still scarce. Finally, as shown in Fig. 5(d), the calculation with $M = 7$ leads to a much improved result: both the vibrational motions and the jetlike dissociation components is clearly observed. Our results indicate that including more orbitals leads to a better description of electron-nuclear correlation, and thus molecular vibrations as well as the dissociative ionization can be well described by the TD-MCSCF method with a sufficient number of orbitals.

Figure 6 shows n -electron ionization probabilities of a quantum-nuclei H_2 molecule. For this calculation, we

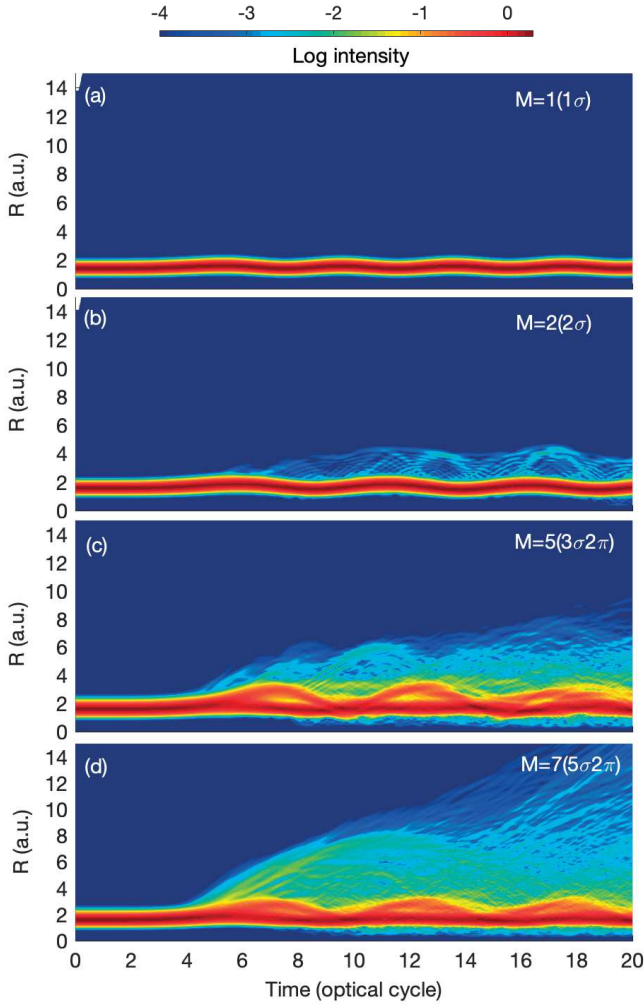


FIG. 5. Time-dependent nuclear probability density of a quantum-nuclei H_2 molecule upon interaction with an infrared laser pulse with a wavelength of 800 nm, an intensity of $3 \times 10^{14} \text{ W/cm}^2$ and a foot-to-foot duration of 8 optical cycles. Same number of electronic and nuclear orbitals M is used: (a) $M = 1$, (b) $M = 2$, (c) $M = 5$, and (d) $M = 7$.

have confirmed that the simulation box is large enough to hold the nuclear density, thus the nuclear coordinate can be safely integrated out. The results converge to that with $M = 7$ (taken as a reference) as the number of orbitals increases. However, quantitatively, the ionization probability differs from that of the clamped-nuclei model (Fig. 3) under the same laser condition. In Fig. 7, we show the single ionization probability of clamped-nuclei H_2 , quantum-nuclei D_2 , and quantum-nuclei H_2 with $M = 7$. It is found that the single ionization probability of quantum-nuclei H_2 is higher than that of D_2 , and both of them are higher than that of clamped-nuclei H_2 . This result suggests the effect of enhanced ionization due to nuclear motion [68, 69].

Figure 8 presents the TD-MCSCF HHG spectra from quantum-nuclei H_2 molecule. The results show an im-

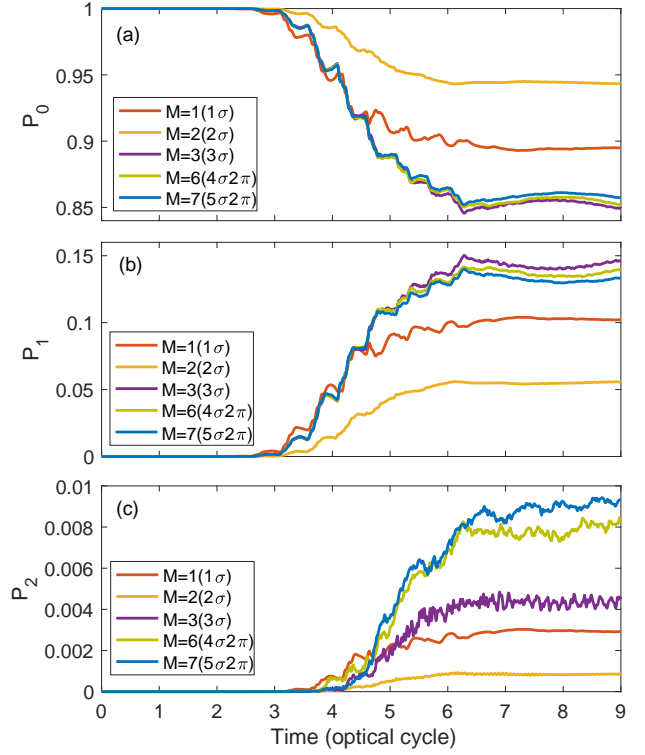


FIG. 6. Time evolution of (a) survival probability, (b) single-ionization probability, and (c) double-ionization probability of a quantum-nuclei H_2 molecule exposed to an infrared laser pulse with a wavelength of 800 nm, an intensity of $3 \times 10^{14} \text{ W/cm}^2$ and a foot-to-foot duration of 8 optical cycles. Results of the TD-MCSCF method are obtained with different numbers of orbitals and same number of electronic and nuclear orbitals M is used.

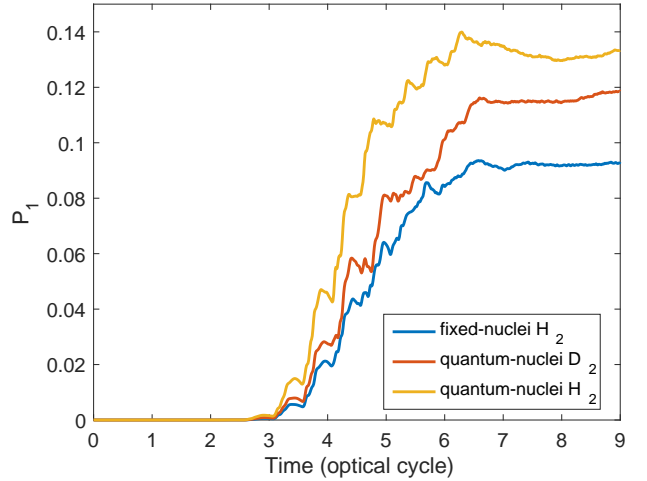


FIG. 7. Time evolution of the single-ionization probability for a clamped-nuclei H_2 molecule, quantum-nuclei D_2 , and quantum-nuclei H_2 . Results of the TD-MCSCF method are obtained with $M = 7$.

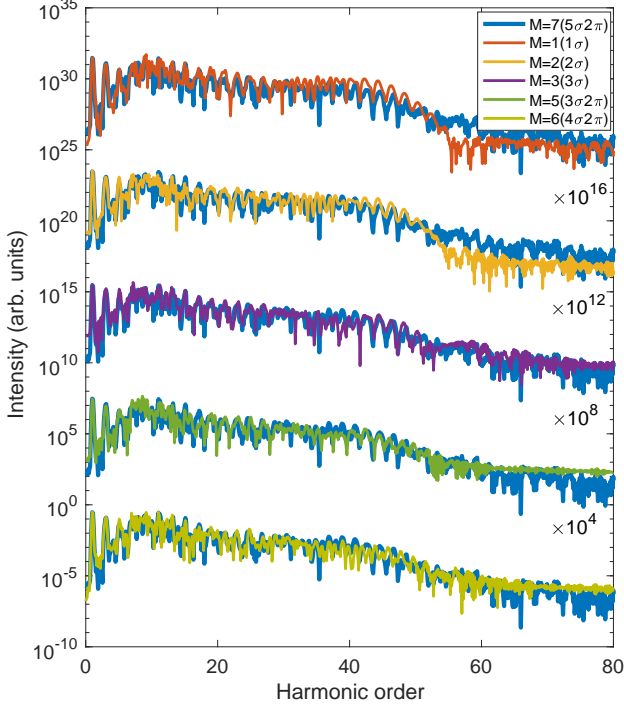


FIG. 8. High-harmonic spectra of a quantum-nuclei H_2 molecule exposed to an infrared laser pulse with a wavelength of 800 nm, an intensity of $3 \times 10^{14} \text{ W/cm}^2$ and a foot-to-foot duration of 8 optical cycles. Same number of electronic and nuclear orbitals M is used. The HHG spectra with different numbers of orbitals are compared to that with $M = 7$.

provement with increasing number of orbitals as in the clamped-nuclei case. However, the harmonic spectrum is not fully converged even with $M = 7$. A similar trend with quantum treatment of nuclei has previously been reported for reduced-dimensional H_2^+ [44]. Nevertheless, the quantitative agreement is already sufficient to address the effects of nuclear motion during the HHG process, as demonstrated below.

Experimentally, it has been observed that high-harmonic emission is stronger in D_2 than that in H_2 due to the faster nuclear motion in the lighter H_2 molecule [70, 71]. We will show that the present TD-MCSCF method, which allows full quantum treatment of nuclei, can well reproduce the experimental results. We consider an 800-nm laser field with a peak intensity of $2 \times 10^{14} \text{ W/cm}^2$. The laser parameters are similar to those in the experiments. In order to reveal the odd order harmonic peaks, we use a multi-cycle laser pulse with total duration of 30 periods. The HHG spectra of quantum-nuclei H_2 and D_2 are calculated with $M = 7$, as shown in Fig. 9(a). Up to the 29th harmonics can be well resolved in the spectra. In Fig. 9(b), the spectra of H_2 and D_2 in the plateau region are plotted on a linear scale. It can be clearly seen that the harmonic signal is stronger

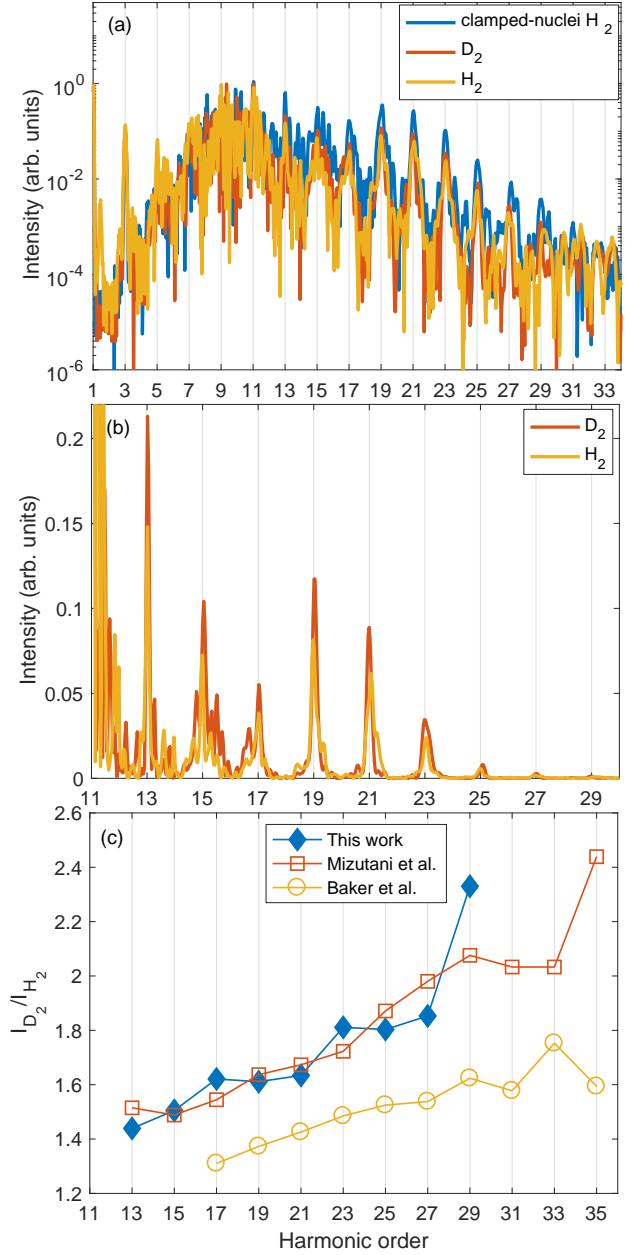


FIG. 9. (a) HHG spectra of quantum-nuclei H_2 (yellow solid line) and D_2 (red solid line) exposed to an infrared laser pulse with a wavelength of 800 nm, an intensity of $2 \times 10^{14} \text{ W/cm}^2$ and a foot-to-foot duration of 30 optical cycles. The HHG spectrum of clamped-nuclei H_2 model (blue solid line) is also presented for comparison. All of the results are calculated by TD-MCSCF method with $M = 7$. In the calculation of D_2 , the nuclear mass is set to 3670.48 a.u. (b) HHG spectra in the plateau region of quantum-nuclei H_2 and D_2 , plotted on a linear scale. (c) The intensity ratios of $I_{\text{D}_2}/I_{\text{H}_2}$ as a function of harmonic order. Experimental data taken from Ref. [70] (yellow open circles) and Ref. [71] (red open squares) are also included.

in D_2 than that in H_2 . Fig. 9(c) shows the intensity ratio between D_2 and H_2 as a function of harmonic order. The ratio is calculated by using the peak values of odd order harmonics. The ratio is larger than unity at all orders and increases with the harmonic order. Our calculation shows quantitative agreement with the experimental measurement in Ref. [71] under the same laser condition. The experimental result from Ref. [70] using a few-cycle laser pulse also exhibits a similar trend, albeit with relatively small values compared to our calculation possibly because of the difference in the laser parameters. The present calculation using the TD-MCSCF method nicely reproduces the experimentally observed isotope effects on HHG, emphasizing the importance of dynamical electron-nuclear correlation during HHG process.

V. SUMMARY

We have presented the numerical implementation of the recently formulated TD-MCSCF method [44] for diatomic molecules in the full-CI expansion. By full quantum treatment of the nuclei, the present implementation allows one to investigate coupled electron-nuclear dynamics of molecules subject to intense laser fields. As a first numerical test, we have applied this method to the ground state as well as the laser-driven dynamics of H_2 molecule. The ground-state properties, including ground-state energy, natural orbitals and natural occupation numbers show remarkable agreement with benchmark data [38] available in the literature, which indicates the correctness of our implementation. For laser-driven dynamics, we have shown that the method can systematically improve the accuracy for describing the highly nonlinear HHG phenomenon by increasing the number of electronic and nuclear orbital functions. Furthermore, the TD-MCSCF method with sufficiently large number of orbitals has been applied to study the isotopic effects of HHG to justify experimental observations. Our results indicate that HHG is sensitive to the laser-induced nuclear vibrational motion. The harmonic emission is more intense in heavier isotopes and the role of nuclear motion in suppressing the intensity of high harmonics is increased with increasing harmonic order.

While the present study has been mainly focused on the electron-nuclear dynamics in HHG, we have also shown that the TD-MCSCF method is capable of describing photoionization and dissociation [37, 72, 73] of molecules interacting with a laser field. In order to properly explain experimental results such as electron-ion coincidence measurements [74, 75] during molecular dissociation, extending the functionality of present implementation to calculate momentum distribution of ionized electron and joint electron-nuclear-energy spectrum will be the further aspects.

ACKNOWLEDGMENTS

Y. L. acknowledges Erik Lötstedt for valuable discussions on propagation methods. This research was supported in part by a Grant-in-Aid for Scientific Research (Grants No. JP18H03891 and No. JP19H00869) from the Ministry of Education, Culture, Sports, Science and Technology (MEXT) of Japan. This research was also partially supported by JST COI (Grant No. JPMJCE1313), JST CREST (Grant No. JPMJCR15N1), and by MEXT Quantum Leap Flagship Program (MEXT Q-LEAP) Grant Number JPMXS0118067246. Y. L. gratefully acknowledges support from JSPS Postdoctoral Fellowships for Research in Japan.

Appendix A: Derivation of natural-orbital constraints

In the TD-MCSCF method, a typical feature is the invariance of the total wave function with respect to time-dependent unitary transformations among the subspace spanned by the occupied orbitals. These unitary transformations give rise to the constraint operators, i.e., $\hat{X}^{(n)}$ and $\hat{X}^{(e)}$, appearing in the EOMs. The natural-orbital representation is one special case, where the one-body RDMs are kept to be diagonal during the time propagation. Taking $\hat{X}^{(e)}$ for example, the natural-orbital constraint matrix can be derived by considering the time derivative of the one-body RDM for electrons

$$\begin{aligned} \frac{d}{dt}(\rho_e)_{\nu}^{\mu} = & \sum_{I,p} \frac{dC_{I,p}^*}{dt} \langle \Phi_I \chi_p | (\hat{E}_e)_{\mu}^{\nu} | \Psi \rangle \\ & + \sum_{I,p} \langle \Psi | (\hat{E}_e)_{\mu}^{\nu} | \Phi_I \chi_p \rangle \frac{dC_{I,p}}{dt}. \end{aligned} \quad (A1)$$

Substituting the CI EOMs Eq. (21) into Eq. (A1) and using the hermiticity of $\hat{X}^{(e)}$ and $\hat{X}^{(n)}$, we get

$$\begin{aligned} \frac{d}{dt}(\rho_e)_{\nu}^{\mu} = & \sum_{I,p} i \langle \Psi | \hat{H} - \hat{X} | \Phi_I \chi_p \rangle \langle \Phi_I \chi_p | (\hat{E}_e)_{\mu}^{\nu} | \Psi \rangle \\ & - \sum_{I,p} i \langle \Psi | (\hat{E}_e)_{\mu}^{\nu} | \Phi_I \chi_p \rangle \langle \Phi_I \chi_p | \hat{H} - \hat{X} | \Psi \rangle, \end{aligned} \quad (A2)$$

where notation $\hat{X} = \hat{X}^{(n)} + \hat{X}^{(e)}$ is used. In the case of full-CI expansion, the configuration projector $\sum_{I,p} |\Phi_I \chi_p\rangle \langle \Phi_I \chi_p|$ can be omitted. The time-derivative of one-body RDM can be rewritten in a compact form employing the commutator $[\hat{a}, \hat{b}] = \hat{a}\hat{b} - \hat{b}\hat{a}$,

$$\begin{aligned} \frac{d}{dt}(\rho_e)_{\nu}^{\mu} = & -i \langle \Psi | [(\hat{E}_e)_{\mu}^{\nu}, \hat{H} - \hat{X}] | \Psi \rangle \\ = & -i \langle \Psi | [(\hat{E}_e)_{\mu}^{\nu}, \hat{H} - \hat{X}^{(e)}] | \Psi \rangle. \end{aligned} \quad (A3)$$

In the natural-orbital representation, $d(\rho_e)_{\nu}^{\mu}/dt = 0$ for $\mu \neq \nu$, and consequently,

$$\langle \Psi | [(\hat{E}_e)_{\mu}^{\nu}, \hat{X}^{(e)}] | \Psi \rangle = \langle \Psi | [(\hat{E}_e)_{\mu}^{\nu}, \hat{H}] | \Psi \rangle. \quad (A4)$$

After some algebraic manipulations to evaluate the commutators, we have

$$(X_e)_\nu^\mu = [(F_e)_\nu^\mu - (F_e^*)_\nu^\mu] \frac{(\rho_e)_\mu^\mu - (\rho_e)_\nu^\nu}{[(\rho_e)_\mu^\mu - (\rho_e)_\nu^\nu]^2 + \epsilon^2}, \quad (\text{A5})$$

with

$$(F_e)_\nu^\mu = \sum_\lambda (h_e)_\lambda^\mu (\rho_e)_\nu^\lambda + \sum_{\lambda p q} (g_{ne})_{q\lambda}^{p\mu} (\rho_{ne})_{p\nu}^{q\lambda} + \sum_{\lambda \gamma \delta} (g_{ee})_{\lambda\delta}^{\mu\gamma} (\rho_{ee})_{\nu\gamma}^{\lambda\delta}, \quad (\text{A6})$$

for off-diagonal matrix elements $\mu \neq \nu$, where ϵ is a small regularization parameter. The constraint does not fix the values of diagonal elements of operator $\hat{X}^{(e)}$, which can be simply set to zero. Same procedures can be applied to the nuclear constraint operators $\hat{X}^{(n)}$, the results are

$$(X_n)_q^p = [(F_n)_q^p - (F_n^*)_q^p] \frac{(\rho_n)_p^p - (\rho_n)_q^q}{[(\rho_n)_p^p - (\rho_n)_q^q]^2 + \epsilon^2}, \quad (\text{A7})$$

with

$$(F_n)_q^p = \sum_r (h_n)_r^p (\rho_n)_q^r + \sum_{r\mu\nu} (g_{ne})_{r\nu}^{p\mu} (\rho_{ne})_{r\nu}^{q\mu}, \quad (\text{A8})$$

for $p \neq q$.

One should note that the above derivations are only valid for real-time propagation. There are differences for the presence of constraint operators between real- and imaginary-time propagation. While the constraint operators are Hermitian in real-time EOMs, they are anti-Hermitian in the imaginary time ones. In the following, we derive the expressions of constraint operators which are suitable for imaginary-time propagation. We use notations $\hat{Y}^{(e)}$ and $\hat{Y}^{(n)}$ as the imaginary-time counterparts for $\hat{X}^{(e)}$ and $\hat{X}^{(n)}$, respectively. By employing a pure imaginary time $t = -i\tau$ with τ being a real variable, the matrix elements of operators $\hat{Y}^{(e)}$ and $\hat{Y}^{(n)}$ are defined as

$$(\hat{Y}_n)_q^p = -\langle \chi_p | \frac{\partial}{\partial \tau} | \chi_q \rangle, \quad (\text{A9})$$

and

$$(\hat{Y}_e)_\nu^\mu = -\langle \psi_\mu | \frac{\partial}{\partial \tau} | \psi_\nu \rangle. \quad (\text{A10})$$

Based on the time-dependent variation principle in imaginary time, we obtain the same EOMs for both CI coefficients and orbitals [Eq. (21)-(23)], except for a replacement $i\frac{\partial}{\partial t} \rightarrow -\frac{\partial}{\partial \tau}$ on the l.h.s of these equations. For instance, The imaginary-time CI EOMs Eq. (xx) read

$$-\frac{d}{d\tau} C_{I,p} = \sum_{J,q} \langle \Phi_I \chi_p | \hat{H} - \hat{Y}^{(n)} - \hat{Y}^{(e)} | \Phi_J \chi_q \rangle C_{J,q}. \quad (\text{A11})$$

Utilizing the anti-Hermiticity of the constraint operators, the complex conjugate of Eq. (A11) is obtained as

$$-\frac{d}{d\tau} C_{I,p}^* = \sum_{J,q} \langle \Phi_J \chi_q | \hat{H} + \hat{Y}^{(n)} + \hat{Y}^{(e)} | \Phi_I \chi_p \rangle C_{J,q}^*. \quad (\text{A12})$$

Substituting Eq. (A11) and (A12) into the time derivative of electronic one-body RDM Eq. (A1) and set the off-diagonal matrix elements to zero, we obtain a relation for $\hat{Y}^{(e)}$ as

$$\langle \Psi | [(\hat{E}_e)_\mu^\nu, \hat{Y}^{(e)}] | \Psi \rangle = \langle \Psi | \{(\hat{E}_e)_\mu^\nu, \hat{H}\} | \Psi \rangle, \quad (\text{A13})$$

where the anti-commutator $\{\hat{a}, \hat{b}\} = \hat{a}\hat{b} + \hat{b}\hat{a}$ is used. Similarly, for nuclear constraint operator $\hat{Y}^{(n)}$, we have

$$\langle \Psi | [(\hat{E}_n)_p^q, \hat{Y}^{(n)}] | \Psi \rangle = \langle \Psi | \{(\hat{E}_n)_p^q, \hat{H}\} | \Psi \rangle. \quad (\text{A14})$$

It is thus interesting to compare Eq. (A13) for time imaginary-time propagation with Eq. (A4) for real-time propagation: the only difference is the replacement of the commutator to the anti-commutator on the r.h.s. of these two equations. The explicit expressions of $\hat{Y}^{(e)}$ and $\hat{Y}^{(n)}$ involve the third-order RDMs, which are tedious and omitted here. The computation of third-order RDMs constitutes a bottleneck for numerical calculations, which needs further investigations. Nevertheless, for an hydrogen molecule with only two electrons and one nuclear degree of freedom used in the present paper, the computational effort is affordable.

Appendix B: The TD-MCSCF formalism for clamped nuclei

In this appendix, we briefly describe the TD-MCSCF method for a multielectron system within the clamped-nuclei model. In the full-CI case, it is equivalent to MCTDHF method. We consider an N -electron diatomic molecule with fixed nuclei in an external laser field. The dynamics of the electronic system is described by the time-dependent Hamiltonian

$$\hat{H}(t) = \hat{H}_1(t) + \hat{H}_2, \quad (\text{B1})$$

with $\hat{H}_1 = \sum_i^N \hat{h}(\mathbf{r}_i, t)$ and

$$\hat{h}(\mathbf{r}, t) = \left(-\frac{\nabla^2}{2} - \sum_{a=1}^2 \frac{Z_a}{|\mathbf{r} - \mathbf{R}_a|} + \hat{V}_{\text{ext}} \right), \quad (\text{B2})$$

$$\hat{H}_2 = \sum_{i=1}^N \sum_{j>i} \frac{1}{|\mathbf{r}_i - \mathbf{r}_j|}, \quad (\text{B3})$$

where laser-electron interaction \hat{V}_{ext} within the dipole approximation either in the LG or in the VG is given by

$$\hat{V}_{\text{ext}}^{\text{LG}}(\mathbf{r}, t) = \mathbf{E}(t) \cdot \mathbf{r}, \quad (\text{B4})$$

$$\hat{V}_{\text{ext}}^{\text{VG}}(\mathbf{r}, t) = -i\mathbf{A}(t) \cdot \nabla. \quad (\text{B5})$$

In the TD-MCSCF method, the N -electron wave function is expressed by a linear combination of Slater determinants as

$$\Psi(t) = \sum_I C_I(t) \Phi(t), \quad (\text{B6})$$

where the Slater determinant $\Phi_I(t)$ is built from M occupied orbitals $\{\psi_\mu(t)\}$. Both the CI coefficients $\{C_I\}$ and the occupied orbitals are time-dependent. By use of time-dependent variational principle, the EOMs are derived to describe the time evolution. The resulting EOMs for the CI coefficients read

$$i \frac{d}{dt} C_I(t) = \sum_J \langle \Psi_I | \hat{H} - \hat{X} | \Psi_J \rangle C_J(t). \quad (\text{B7})$$

The EOMs for the orbitals are given by

$$i \frac{\partial}{\partial t} |\psi_i\rangle = \hat{Q} \left\{ \hat{h} |\psi_i\rangle + \sum_{\mu, \nu, \lambda, \gamma} (D^{-1})_i^\mu P_{\mu\lambda}^\nu \hat{W}_\gamma^\lambda |\psi_\nu\rangle \right\} + \sum_j |\psi_j\rangle (X)_i^j, \quad (\text{B8})$$

where $\hat{Q} = 1 - \sum_\mu |\psi_\mu\rangle \langle \psi_\mu|$ is the projector against the occupied orbital space, D and P the one- and two-electron RDMs, \hat{W}_ν^μ the mean-field potential with the same definition as in Eq. (24), and \hat{X} the constraint operator defined in Eq. (28). Here we also use the natural-orbital constraint \hat{X} as derived in Appendix A.

Appendix C: Modification of ETDRK2 method with a time-dependent stiff part

Following Ref. [58], it is possible to generalize the ETD method to treat

$$\frac{\partial}{\partial t} u(t) = -i\hat{h}(t)u(t) + N[t, u(t)], \quad (\text{C1})$$

where the operator $\hat{h}(t)$ is time-dependent and chosen to be the one-electron Hamiltonian $\hat{h}(t) = \hat{h}^{(e)}(t)$. Within the time interval $[t_n, t_{n+1}]$, we rewrite the operator $\hat{h}(t)$ as

$$\hat{h}(t) = \hat{h}(t_n) + \dot{\hat{h}}(t_n)(t - t_n) + [\hat{h}(t) - \hat{h}(t_n)] - \dot{\hat{h}}(t_n)(t - t_n), \quad (\text{C2})$$

where $\dot{\hat{h}}(t) = \partial \hat{h}(t) / \partial t$. By introducing an auxiliary vector $\mathcal{U}(t) = [t - t_n, u(t)]^T$ and employing Eq. (C2), we can rewrite Eq. (C1) coupled with $\dot{t} = 1$ as

$$\frac{\partial}{\partial t} \mathcal{U}(t) = -i\mathcal{H}\mathcal{U}(t) + \mathcal{N}(t), \quad (\text{C3})$$

with

$$\mathcal{H} = \begin{bmatrix} 0 & 0 \\ \dot{\hat{h}}(t_n)u(t_n) & \hat{h}(t_n) \end{bmatrix}, \quad \mathcal{N}(t) = \begin{bmatrix} 1 \\ N'[t, u(t)] \end{bmatrix}, \quad (\text{C4})$$

where

$$N'[t, u(t)] = N[t, u(t)] - i [\hat{h}(t) - \hat{h}(t_n)] u(t) + i\dot{\hat{h}}(t_n)(t - t_n)u(t_n). \quad (\text{C5})$$

It is obvious that \mathcal{H} is now time-independent, thus the ETD method with the time-independent linear operator can be applied to Eq. (C3). The φ -functions of \mathcal{H} are give by

$$\varphi_k(-i\mathcal{H}\Delta t) = \begin{bmatrix} \varphi_k(0) & 0 \\ -i\Delta t \varphi_{k+1}(-i\dot{\hat{h}}(t_n)\Delta t)\dot{\hat{h}}(t_n)u(t_n) & \varphi_k(-i\hat{h}(t_n)\Delta t) \end{bmatrix}. \quad (\text{C6})$$

The final expressions for ETDRK2 method are

$$a(t_n) = u(t_n) + \Delta t \varphi_1(-i\dot{\hat{h}}(t_n)\Delta t) \left\{ N[t_n, u(t_n)] - i\dot{\hat{h}}(t_n)u(t_n) \right\} - i\Delta t^2 \varphi_2(-i\dot{\hat{h}}(t_n)\Delta t)\dot{\hat{h}}(t_n)u(t_n), \quad (\text{C7})$$

and

$$u(t_{n+1}) = a(t_n) + \Delta t \varphi_2(-i\dot{\hat{h}}(t_n)\Delta t) \left\{ W[t_{n+1}, a(t_n)] - W[t_n, u(t_n)] - i\{\hat{h}(t_{n+1}) - \hat{h}(t_n)\}a(t_n) + i\Delta t \dot{\hat{h}}(t_n)u(t_n) \right\}. \quad (\text{C8})$$

-
- [1] M. Hentschel, R. Kienberger, C. Spielmann, G. A. Reider, N. Milosevic, T. Brabec, P. Corkum, U. Heinzmann, M. Drescher, and F. Krausz, *Nature* **414**, 509 (2001).
- [2] P.-M. Paul, E. S. Toma, P. Breger, G. Mullot, F. Augé, P. Balcou, H. G. Muller, and P. Agostini, *Science* **292**, 1689 (2001).
- [3] M. Chini, K. Zhao, and Z. Chang, *Nature Photonics* **8**, 178 (2014).
- [4] I. Pupeza, D. Sánchez, J. Zhang, N. Lilienfein, M. Seidel, N. Karpowicz, T. Paasch-Colberg, I. Znakovskaya, M. Pescher, W. Schweinberger, *et al.*, *Nature Photonics* **9**, 721 (2015).
- [5] T. Popmintchev, M.-C. Chen, D. Popmintchev, P. Arpin, S. Brown, S. Ališauskas, G. Andriukaitis, T. Balčiunas, O. D. Mücke, A. Pugzlys, *et al.*, *science* **336**, 1287 (2012).
- [6] P. Agostini and L. F. DiMauro, *Reports Prog. Phys.* **67**, 813 (2004).
- [7] F. Krausz and M. Ivanov, *Rev. Mod. Phys.* **81**, 163 (2009).
- [8] P. á. Corkum and F. Krausz, *Nature physics* **3**, 381 (2007).
- [9] L. Gallmann, C. Cirelli, and U. Keller, *Annu. Rev. Phys. Chem.* **63**, 447 (2012).
- [10] F. Calegari, D. Ayuso, A. Trabattini, L. Belshaw, S. De Camillis, S. Anumula, F. Frassetto, L. Poletto, A. Palacios, P. Decleva, *et al.*, *Science* **346**, 336 (2014).
- [11] M. Nisoli, P. Decleva, F. Calegari, A. Palacios, and F. Martín, *Chemical reviews* **117**, 10760 (2017).
- [12] T. T. Luu, M. Garg, S. Y. Kruchinin, A. Moulet, M. T. Hassan, and E. Goulielmakis, *Nature* **521**, 498 (2015).
- [13] M. Hohenleutner, F. Langer, O. Schubert, M. Knorr, U. Huttner, S. W. Koch, M. Kira, and R. Huber, *Nature* **523**, 572 (2015).
- [14] S. Ghimire, A. D. DiChiara, E. Sistrunk, P. Agostini, L. F. DiMauro, and D. A. Reis, *Nature physics* **7**, 138 (2011).
- [15] A. J. Uzan, G. Orenstein, Á. Jiménez-Galán, C. McDonald, R. E. Silva, B. D. Bruner, N. D. Klimkin, V. Blanchet, T. Arusi-Parpar, M. Krüger, *et al.*, *Nature Photonics* **14**, 183 (2020).
- [16] F. Lépine, M. Y. Ivanov, and M. J. Vrakking, *Nature Photonics* **8**, 195 (2014).
- [17] P. Ranitovic, C. W. Hogle, P. Rivière, A. Palacios, X.-M. Tong, N. Toshima, A. González-Castrillo, L. Martín, F. Martín, M. M. Murnane, *et al.*, *Proceedings of the National Academy of Sciences* **111**, 912 (2014).
- [18] J. Zanghellini, M. Kitzler, C. Fabian, T. Brabec, and A. Scrinzi, *LASER PHYSICS-LAWRENCE-* **13**, 1064 (2003).
- [19] T. Kato and H. Kono, *Chemical physics letters* **392**, 533 (2004).
- [20] J. Caillat, J. Zanghellini, M. Kitzler, O. Koch, W. Kreuzer, and A. Scrinzi, *Physical review A* **71**, 012712 (2005).
- [21] M. Nest, T. Klamroth, and P. Saalfrank, *The Journal of chemical physics* **122**, 124102 (2005).
- [22] K. Ishikawa and T. Sato, *IEEE J. Sel. Top. Quantum Electron.* , 1 (2015).
- [23] A. U. Lode, C. Lévéque, L. B. Madsen, A. I. Streltsov, and O. E. Alon, *Reviews of Modern Physics* **92**, 011001 (2020).
- [24] T. Sato and K. L. Ishikawa, *Phys. Rev. A* **88**, 023402 (2013).
- [25] T. Sato, K. L. Ishikawa, I. Březinová, F. Lackner, S. Nagele, and J. Burgdörfer, *Phys. Rev. A* **94**, 023405 (2016).
- [26] Y. Orimo, T. Sato, A. Scrinzi, and K. L. Ishikawa, *Phys. Rev. A* **97**, 023423 (2018).
- [27] T. Sato and K. L. Ishikawa, *Phys. Rev. A* **91**, 023417 (2015).
- [28] Y. Orimo, T. Sato, and K. L. Ishikawa, *Physical Review A* **100**, 013419 (2019).
- [29] D. J. Haxton and C. W. McCurdy, *Phys. Rev. A* **91**, 012509 (2015).
- [30] H. Miyagi and L. B. Madsen, *Physical Review A* **87**, 062511 (2013).
- [31] H. Miyagi and L. B. Madsen, *Phys. Rev. A* **89**, 063416 (2014).
- [32] M. Nest, *Chemical Physics Letters* **472**, 171 (2009).
- [33] I. S. Ulusoy and M. Nest, *The Journal of chemical physics* **136**, 054112 (2012).
- [34] L. E. Aebersold, I. S. Ulusoy, and A. K. Wilson, *Physical Review A* **100**, 023406 (2019).
- [35] T. Kato and K. Yamanouchi, *The Journal of chemical physics* **131**, 164118 (2009).
- [36] Y. Ide, T. Kato, and K. Yamanouchi, *Chemical Physics Letters* **595**, 180 (2014).
- [37] E. Lötstedt, T. Kato, and K. Yamanouchi, *Physical Review A* **99**, 013404 (2019).
- [38] D. J. Haxton, K. V. Lawler, and C. W. McCurdy, *Physical Review A* **83**, 063416 (2011).
- [39] D. J. Haxton, K. V. Lawler, and C. W. McCurdy, *Physical Review A* **91**, 062502 (2015).
- [40] O. E. Alon, A. I. Streltsov, and L. S. Cederbaum, *Physical Review A* **76**, 062501 (2007).
- [41] O. E. Alon, A. I. Streltsov, and L. S. Cederbaum, *The Journal of chemical physics* **127**, 154103 (2007).
- [42] O. E. Alon, A. I. Streltsov, and L. S. Cederbaum, *Physical Review A* **79**, 022503 (2009).
- [43] O. E. Alon, A. I. Streltsov, K. Sakmann, A. U. Lode, J. Grond, and L. S. Cederbaum, *Chemical Physics* **401**, 2 (2012).
- [44] R. Anzaki, T. Sato, and K. L. Ishikawa, *Physical Chemistry Chemical Physics* **19**, 22008 (2017).
- [45] J. R. Hiskes, *Physical Review* **122**, 1207 (1961).
- [46] R. T. Pack and G. A. Parker, *The Journal of chemical physics* **87**, 3888 (1987).
- [47] A. Palacios, J. L. Sanz-Vicario, and F. Martín, *Journal of Physics B: Atomic, Molecular and Optical Physics* **48**, 242001 (2015).
- [48] P.-O. Löwdin and P. Mukherjee, *Chemical Physics Letters* **14**, 1 (1972).
- [49] R. Moccia, *International Journal of Quantum Chemistry* **7**, 779 (1973).
- [50] M. H. Beck, A. Jäckle, G. A. Worth, and H.-D. Meyer, *Physics reports* **324**, 1 (2000).
- [51] P.-O. Löwdin, *Physical Review* **97**, 1474 (1955).
- [52] D. Hochstuhl and M. Bonitz, *The Journal of chemical physics* **134**, 084106 (2011).
- [53] R. Sawada, T. Sato, and K. L. Ishikawa, *Phys. Rev. A* **93**, 023434 (2016).
- [54] F. Gygi, *Phys. Rev. B* **51**, 11190 (1995).

- [55] G. Zumbach, N. Modine, and E. Kaxiras, *Solid State Commun.* **99**, 57 (1996).
- [56] D. Dundas, *J. Chem. Phys.* **136**, 194303 (2012).
- [57] D. Kidd, C. Covington, and K. Varga, *Physical Review E* **96**, 063307 (2017).
- [58] M. Hochbruck and A. Ostermann, *Acta Numer.* **19**, 209 (2010).
- [59] C. W. McCurdy, C. K. Stroud, and M. K. Wisinski, *Phys. Rev. A* **43**, 5980 (1991).
- [60] A. Scrinzi, *Phys. Rev. A* **81**, 053845 (2010).
- [61] C. W. McCurdy, M. Baertschy, and T. N. Rescigno, *J. Phys. B At. Mol. Opt. Phys.* **37**, R137 (2004).
- [62] D. A. Telnov, K. E. Sosnova, E. Rozenbaum, and S.-I. Chu, *Phys. Rev. A* **87**, 053406 (2013).
- [63] R. B. Sidje, *ACM Transactions on Mathematical Software (TOMS)* **24**, 130 (1998).
- [64] X. Guan, K. Bartschat, and B. I. Schneider, *Physical Review A* **83**, 043403 (2011).
- [65] S. Bubin and L. Adamowicz, *The Journal of chemical physics* **118**, 3079 (2003).
- [66] T. Sato and K. L. Ishikawa, *Journal of Physics B: Atomic, Molecular and Optical Physics* **47**, 204031 (2014).
- [67] E. Lötstedt, T. Szidarovszky, F. H. Faisal, T. Kato, and K. Yamanouchi, *Journal of Physics B: Atomic, Molecular and Optical Physics* **53**, 105601 (2020).
- [68] E. Dehghanian, A. D. Bandrauk, and G. L. Kamta, *Physical Review A* **81**, 061403 (2010).
- [69] S. Chattopadhyay and L. B. Madsen, *Physical Review A* **99**, 023424 (2019).
- [70] S. Baker, J. S. Robinson, C. Haworth, H. Teng, R. Smith, C. Chirilă, M. Lein, J. Tisch, and J. P. Marangos, *Science* **312**, 424 (2006).
- [71] H. Mizutani, S. Minemoto, Y. Oguchi, and H. Sakai, *Journal of Physics B: Atomic, Molecular and Optical Physics* **44**, 081002 (2011).
- [72] F. Martín, J. Fernández, T. Havermeier, L. Foucar, T. Weber, K. Kreidi, M. Schöffler, L. Schmidt, T. Jahnke, O. Jagutzki, *et al.*, *Science* **315**, 629 (2007).
- [73] L. Cattaneo, J. Vos, R. Y. Bello, A. Palacios, S. Heuser, L. Pedrelli, M. Lucchini, C. Cirelli, F. Martín, and U. Keller, *Nature Physics* **14**, 733 (2018).
- [74] R. Dörner, V. Mergel, O. Jagutzki, L. Spielberger, J. Ullrich, R. Moshhammer, and H. Schmidt-Böcking, *Physics Reports* **330**, 95 (2000).
- [75] J. Ullrich, R. Moshhammer, A. Dorn, R. Dörner, L. P. H. Schmidt, and H. Schmidt-Böcking, *Reports on Progress in Physics* **66**, 1463 (2003).